2024 International Conference on Science, Engineering and Business for Driving Sustainable Development Goals (SEB4SDG) | 979-8-3503-5815-5/24/$31.00 ©2024 IEEE | DOI: 10.1109/SEB4SDG60871.2024.10629820

3D mmWave MIMO Channel Modeling and Reconstruction for Street Canyon and Highrise Scenarios

Olabode Idowu-Bismark
Dept of Electrical and Information Engineering
Covenant University
Ota, Nigeria
https://orcid.org/0000-0002-7958-1121

Oluwadamilola Oshin
Dept of Electrical and Information Engineering
Covenant University
Ota, Nigeria
damilola.oshin@covenantuniversity.edu.ng

Emmanuel Adetiba
Dept of Electrical and Information Engineering
Covenant University
Ota, Nigeria
emmanuel.adetiba@covenantuniversity.edu.ng

Oluwatobiloba Idowu-Bismark
Department of Computer Science,
University of Hertfordshire,
AL109JD Welwyn Hatfield,
United Kingdom
bismarktobi@yahoo.com

***Abstract*—The use of millimeter-wave (mmWave) and full-dimensional multiple-input multiple-output (FD-MIMO) antenna systems for 3D wireless communication is being exploited for enhanced network capacity improvement in the ongoing fifth-generation (5G) deployment. For adequate assessment of competing air interface, random access channelization, and beam alignment procedures in mmWave systems, channel models for different use scenarios are necessary. A ray-tracing study was conducted with the use of a Wireless Insite ray tracing algorithm to characterize the mmWave channel in urban areas, using Lagos Island, Nigeria databases to predict measured statistics. These statistics include path loss, rms delay spread, angular spread of arrival, and departure in the azimuth and elevation domain. A 3GPP-style 3D mmWave channel is modeled and reconstructed, emphasizing the use of a ray tracer to determine elevation model parameters. Line of sight (LOS) and non-line of sight (NLOS) 3D models were developed for street canyon and high-rise scenarios**

Keywords—5G, mmWave Massive MIMO, Channel Reconstruction, Wireless Insite

I. INTRODUCTION (*HEADING 1*)

The volatile constantly-increasing appetite for mobile traffic as everyone's desire for online presence, such as Facebook, Twitter, and video streaming [1], has led to the evolution of the Long Term Evolution (LTE) into the LTE-Advance without being able to meet the ever-growing demand for mobile data. The above condition necessitates the introduction of the 5G network. Network Densification (ND) has been suggested as a method to meet the data rate requirement of the 5G [2] [3]. ND is the unification of spatial densification and spectral aggregation. Spatial densification is the deployment of small cells (Picocells, Femtocells) as an overlay in macrocells and the use of massive multiple-input and multiple-output (MIMO) at the base station [4]. Spectral aggregation uses large carrier frequencies spanning 500 MHz to the mmWave (30 GHz – 300 GHz) band.

The second major technology for obtaining a higher data rate and ultra-reliable low-latency communication is the millimeter-wave band [5]. However, mmWave signals are easily blocked by obstacles preventing direct Line-of-Sight (LOS) communications. Also, the increased diffraction loss at mmWave results in deep shadow regions, degrading the propagation performance [6]. The above makes the mmWave channel seem very volatile to mobile users. It is, therefore, necessary to find a modeling strategy suitable for the mmWave channel. In order to sufficiently evaluate contending air interfaces and beam alignment protocols for mmWave communications, various case scenarios exist for which a realistic assemblage of channel models must be produced. These channel models are required with features similar to the 3D channel model developed in the 3rd Generation Partnership Project (3GPP) [7] including pathloss, distant-dependent rms delay spread, and distant-dependent azimuth/elevation angle spreads of departure and arrival.

In channel modeling and reconstruction, the channel matrix otherwise called the channel impulse response contains all the channel multipath components of interest that are needed to model the channel. Assuming N clusters of multipath rays from scatterers exist between the base station and the receiver where each cluster is made up of one resolvable propagation path and delay τ. Let the complex envelope of the transmitted single input single output (SISO) signal (baseband signal) be represented as $\tilde{S}(t)$ while the real part of the transmitted bandpass signal $S(t)$ is:

$$S(t) = Re\left[\tilde{S}(t)e^{j2\pi f_c t}\right] \quad (1)$$

where the signal phase is given as $j2\pi f_c t$. The received passband signal thus becomes:

$$r(t) = Re\left[\sum_{l=1}^{L} \alpha_l e^{j\emptyset_l(t)}\tilde{S}(t-\tau_l)e^{j2\pi f_c t}\right] \quad (2)$$

where the received baseband signal is given as:

$$\tilde{r}(t) = \sum_{l=1}^{L} \alpha_l e^{j\emptyset_l(t)}\tilde{S}(t-\tau_l) \quad (3)$$

Substituting Equation (3) into Equation (2), thus:

$$r(t) = Re[\tilde{r}(t)e^{j2\pi f_c t}] \quad (4)$$

Every transmitted signal through the propagation channel experiences attenuation and delay termed its channel impulse response. The impulse response for the l^{th} MPC can be extracted from (3) as in [8]:

$$h(t,\tau_l) = \alpha_l e^{j\emptyset_l(t)} \quad (5)$$

Substituting Equation (5) into Equation (3), we have Equation (6) as:

$$\tilde{r}(t) = \sum_{l=1}^{L} h(t,\tau_l)\tilde{S}(t-\tau_l) \quad (6)$$

Using the convolution principle, Equation (6) becomes:

$$\tilde{r}(t) = h(t,\tau) * \tilde{S}(t) \quad (7)$$

where the channel impulse response is given as:

$$h(t,\tau) = \sum_{l=1}^{L} h(t,\tau_l).\delta(t-\tau_l) \quad (8)$$

Equation (8) is a 2D channel model and can be extended to a 3D model by including the elevation angles at the arrival and departure. A general CIR time-domain model can then be written as in [9]:

$$h(\tau,\theta) = \sum_{l=1}^{L} h(t,\tau_l).\delta(t-\tau_l).\delta(\theta-\theta_l) \quad (9)$$

where $\delta(t-\tau_l)$ is the time of arrival impulse, and $\delta(\theta-\theta_l)$ is the angle of arrival impulse from where channel parameters such as delay spread, angular spread, etc. can be calculated. Equation (9) can be expanded into equation (10) as in [10]:

$$\boldsymbol{H}^{3D}_{n_{sbs},n_{mbs},n}(t) = \sqrt{P}_n \sum_{l=1}^{L} \begin{bmatrix} F_{rx,n_{sbs},V}(\varphi_{l,n},\vartheta_{l,n}) \\ F_{rx,n_{sbs},H}(\varphi_{l,n},\vartheta_{l,n}) \end{bmatrix}^T . \begin{bmatrix} e^{j\Phi^{vv}_{l,n}} & \sqrt{\mathfrak{k}^{-1}_{l,n}}e^{j\Phi^{vh}_{l,n}} \\ \sqrt{\mathfrak{k}^{-1}_{l,n}}e^{j\Phi^{hv}_{l,n}} & e^{j\Phi^{hh}_{l,n}} \end{bmatrix} . \begin{bmatrix} F_{tx,n_{mbs},V}(\phi_{l,n},\theta_{l,n}) \\ F_{tx,n_{mbs},H}(\phi_{l,n},\theta_{l,n}) \end{bmatrix} . exp\{j2\pi\lambda^{-1}(\bar{\varphi}_{l,n}.\bar{\boldsymbol{d}}_{rx,n_{sbs}})\} . exp\{j2\pi\lambda^{-1}(\bar{\phi}_{l,n}.\bar{\boldsymbol{d}}_{tx,n_{mbs}})\} \quad (10)$$

Where the azimuth angle of departure and arrival is represented by $\phi_{l,n}$, and $\varphi_{l,n}$. In contrast, the elevation angle of departure and arrival are represented by $\theta_{l,n}$, and $\vartheta_{l,n}$, respectively. $F_{rx,n_{sbs},V}$ and $F_{rx,n_{sbs},H}$ is the small cell (sbs^{th}) field antenna patterns in 3D for the theta (vertical, V) and phi (horizontal, H) polarizations, respectively. $\Phi^{vv}_{l,n}$ is the phase value for the vv (vertical-vertical) polarization, while the other three are for $vh, hv,$ and hh polarization combinations. The spherical unit vector in the direction of azimuth and elevation angles of departure and arrival are represented by $\bar{\varphi}_{l,n}$, and $\bar{\phi}_{l,n}$, respectively. $\bar{\boldsymbol{d}}_{rx,n_{sbs}}$, and $\bar{\boldsymbol{d}}_{tx,n_{mbs}}$ are the location vector of received small cell antenna element n_{sbs} and transmit antenna element. n_{mbs}, respectively with $\mathfrak{k}$ being the cross-polarization power ratio in a linear scale and P_n is the power of cluster (n).

Identify the applicable funding agency here. If none, delete this text box.

II. Literature Review

Various channel models and channel reconstruction were proposed for mmWave communications, including [11] which was carried out at 32 GHz for the indoor office environment. In a much earlier model, the authors of [12] developed a model for a street canyon environment at 70 – 80 GHz band, since the work was limited to the Azimuth domain, it was improved upon in the [13] where a 3D ray tracing technique was used to extend it to 3D by including elevation spread for use in system level simulation. The work of [7] improved the work of [13] by extending its application to non-line-of-sight links, polarization, and angle biases. The authors of [14] presented a set of mmWave radio propagation parameters based on both measurement and ray-tracing techniques. The author of [15] used limited received signal strength (RSS) measurement to reconstruct the BS-to-ground channel. The authors of [16] used a compressive sensing technique for data recovery in an embedded system. In the 6G domain where Intelligent Reflecting Surfaces (IRSs) are used for improved data rates in mmWave and terahertz systems, the author of [17] combines low-rank matrix with subspace side information that exploits sparsity for channel reconstruction.

Given the emerging field of mmWave wireless communication, there currently is a gap in measurements, including the lack of extensive and detailed elevation statistics especially for angle of departure at the base station. In this paper, we advocate a mmWave channel model that attempts to improve on the channel model in [14] by concentrating on characterizing mmWave propagation models including both 3D angular and delay domain channel parameters to develop a double-directional wideband channel model in the 28 GHz band for both the street canyon and high-rise scenarios of Lagos island, Nigeria. Using the 3D LTE toolbox in MATLAB, we reconstructed bi-directional channel models in the context of urban canyons and high rise in the 28 GHz mmWave band as our key finding. The research objective of this work is therefore to develop and reconstruct 3GPP-similar LOS/NLOS channel models for the street canyon scenario and the high-rise scenario in Lagos Island Nigeria.

III. Methodology

The research method used in this work is to achieve the purpose of channel parameter extraction needed to model and reconstruct the channels. The Wireless Insite ray tracing simulation algorithm was used. The simulations were conducted in a virtual environment, using the digital map of Lagos Island, Nigeria, with dimensions 500m x 500m. The transmitter is located a bit offset from the middle of the coverage area. Two typical scenarios are considered: outdoor-to-indoor (O2I) high-rise and urban microcell (UMi) street canyon scenarios. In the UMi Street Canyon scenario, the receivers are positioned along Broad Street at 2.5 m elevation from the ground with 1 m space etween each receiver along the street. The total number of receivers deployed is 600. The BS is equipped with a 32 MIMO transmitter antenna and uses maximum ratio transmission (MRT) beamforming with adaptive modulation. In contrast,

each small cell is equipped with a 4 MIMO receiver antenna and uses maximum ratio combining (MRC) for signal detection. Figure 1 is the digital 3D map of the virtual environment and Table 1 shows the simulation parameters

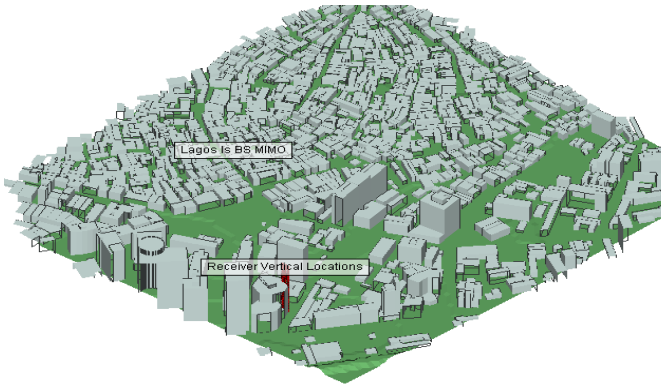

Figure 1: Digital 3D Map of the Virtual Environment of Data Collection

TABLE I. SIMULATION PARAMETERS

Simulation Parameters	Values
Street Canyon small cells number	600
High-rise small cells number	30
Operating Frequency	28 GHz
Signal Bandwidth	100 MHz
Base Station Transmit power	30 dBm
Base Station height	10m
Small cell height: Street	2.5m
Small cell height: High-rise	various
Base Station Antenna	4 x 4 UPA
Small cell antenna	2 x 2
Antenna element spacing	1
Max reflection number	6
Max diffraction number	1
Max penetration number	1

In creating the propagation environment, a 3D geometric digital map is loaded onto the Wireless Insite ray tracing engine for the simulation to obtain MIMO channel parameters. The dataset of each parameter is imported to MATLAB, 2017b. The statistics of the PDF of each parameter that modeled their behavior are then used in the 3D LTE toolbox to reconstruct the models

IV. RESULT AND DISCUSSIONS

A. RMS Delay Spread Distance Dependency Model

When the RMS DS values were plotted against distance, it was shown that the RMS DS increases linearly as distance increases up to 200 m.. The above is evident since a street canyon location behaves like a waveguide to the signal being transmitted. Equation (11) represents the RMS DS distance dependency model. A linear relationship has also been established between RMS DS and path loss [18].

$$RMSDS_{StreetCanyon} = 0.4d + 25.41 \qquad (11)$$

where (meters) is the distance between the base station and the receivers.

When the RMS delay spread was simulated and the results were plotted against the building height, for the high-rise scenario, we observed multiple arriving cluster where the different MPCs of different clusters arrived at different set of small cells. It was noticed that the MPCs of clusters 2 and 3 take longer routes thus having longer delay time of arrival. The RMS DS distance dependency model for the high-rise is thus given by equation (12).

$$RMSDS_{Highrise} = 0.61n^2 - 6.99n + 100 \qquad (12)$$

Where is the building floor number (A floor is 3.5m high)

B. RMS Delay Spread Model

The RMS DS of the street canyon has a normal PDF distribution. The arriving MPCs are from a single cluster. The MPCs are from three different clusters for the high-rise, resulting in three peaks for the RMS DS. They are free of each other and fitted by either normal or lognormal distribution. It has been recognized that DS features depend significantly on the signal bandwidth and the environment where it propagates rather than the carrier frequency [19]. The model of RMS DS for the street canyon scenario is shown as equation (13) using the distribution statistics.

$$f(DS)_{Street} = \frac{1}{14.44} e^{\frac{-(DS-40.98)^2}{66.36}} \qquad (13)$$

MPCs reaching the high-rise are mostly from NLOS directions due to blocking structures, with little or no LOS rays. Therefore, the rays arriving at the small cells mainly come from several reflections of neighboring high-rise structures and low-rise rooftops. The above is an expected outcome for a dense high-rise environment [20]. The distribution of the RMS DS for the high-rise is thus modeled as follows. The first arriving cluster has a normal distribution, while the second and third arriving clusters have a lognormal distribution. Using the statistics of the various distribution fits, their models are given as equations (14), (15), and (16).

$$f(DS)_{Highrise1} = \frac{1}{51.71} e^{-\frac{(DS_{HR1} - 69.05)^2}{851.19}} \qquad (14)$$

where RMS DS HR_1 in equation (20) represents the RMS delay spread for the first arriving cluster. The second arriving cluster has a Lognormal distribution.

$$f(DS)_{Highrise2} = \frac{1}{0.25 DS_{HR2}} e^{-\frac{(\log_{10} DS_{HR2} - 5.39)}{0.02}} \qquad (15)$$

where RMS DS HR_2 in equation (21) represents the RMS delay spread for the second arriving cluster. The third arriving cluster has a Lognormal distribution.

$$f(DS)_{Highrise3} = \frac{1}{0.16 DS_{HR3}} e^{-\frac{(\log_{10} DS_{HR3} - 5.95)}{0.0079}} \qquad (16)$$

where RMS DS HR_3 in equation (16) represents the delay spread for the third arriving cluster.

C. RMS Angular Spread Distance Dependency Modeling

According to Almesaeed et al. (2017) [21], propagation measurement has shown that multipath components arriving at a receiver from over-the-rooftop and in a high-rise propagation environment tend to have a higher elevation angle spread compared to MPC from corridor-like (wave-guided) street canyons.

It is observed that the ground reflections of the elevation rays in the near LOS situation led to the decrease of elevation spread for both arrival (ESA) and departure (ESD) rays as distance increases from the BS for the street canyon scenario. Here, the SC's distance from the BS increases, causing a decrease in the angle between the reflection direction and the near LOS direction. Thus, the ESA and ESD, whose values depend on these angles' interplay, decrease with the distance between the BS and small cells. The RMS ESA/ESD distance dependency relationship shows an exponential curve with the models represented by equation (17) and (18)

$$f(x)_{RMSESA} = 41.35e^{-0.15x} + 2.56e^{-0.0025x} \quad (17)$$

$$f(x)_{RMSESD} = 28.93e^{-0.108x} + 0.436e^{-0.0022x} \quad (18)$$

A scatter plot of RMS ASA and RMS ASD values against distance reveals a zigzag behavior of the RMS ASA/ASD as the distance increases as their values match the street structural construction and physical outlay changes.

Plotting the RMS ESA and RMS ESD values against distance reveals a linear relationship as ESA and ESD increase with the height of the building. The distance dependency model for high-rise RMS ESA is thus represented by equation (19) and RMS ESD by equation (20)

$$f(d)_{RMSESA} = -0.005d^2 + 0.72d - 1.37 \quad (19)$$

$$f(d)_{RMSESD} = 1.59d - 4.90 \quad (20)$$

The RMS ASA and RMS ASD values plotted against distance show a negative linear relationship, where ASA decreases with distance while ASD increases with distance and the RMS ASA/ASD distance dependency models are given by equations (21) and (22)

$$f(x)_{RMSASA} = -5.46x + 36.76 \quad (21)$$

$$f(x)_{RMSASD} = 1.076x + 21.44 \quad (22)$$

D. Angular Spread Modeling

This section uses the same dataset used for distance dependency modeling to model the parameters' pdf. Five hundred and ninety-six samples of ASA, ESA, ASD, and ESD are used for the street scenario, and 30 samples for the high-rise scenario. RMS ESA and ESD distributions in the high-rise and Street canyon scenarios show lognormal distribution. The general model for the angular spread in the elevation domain for both scenarios is given by equation (23).

$$f_\theta = \frac{1}{\theta\sigma\sqrt{2\pi}} e^{\frac{-(ln\theta-\mu)^2}{2\sigma^2}} \quad (23)$$

Where the elevation domain parameter is represented by θ, the inclusion of the distribution statistics (μ_{ESA},μ_{ESD}, σ_{ESA}, and σ_{ESD}) for each RMS ESA or RMS ESD in the equation for the respective scenario will make the model specific to it. RMS ASA/ASD in both scenarios also follows the lognormal distribution. the general model for the angular spread in the azimuth domain for both scenarios is given by equation (24)

$$f_\varphi = \frac{1}{\varphi\sigma\sqrt{2\pi}} e^{\frac{-(ln\varphi-\mu)^2}{2\sigma^2}} \quad (24)$$

Where the azimuth domain parameter is represented by φ, including the distribution statistics (μ_{ASA},μ_{ASD},σ_{ASA}, and σ_{ASD}) for each angular spread in the equation will make the model specific.

E. Reconstruction Method for 3D Channel Model

Based on the ray-tracing data and obtained parameter values, we propose a mmWave channel model for the street canyon and the high-rise scenarios reconstructed using the procedures outlined in 3GPP TR 36.873 release 12 [22]. The steps are detailed below:

1. Set up simulation environment using the 3D digital map of Lagos Island in Wireless Insite ray-tracing engine (determine SBS and MBS location, antenna array configuration, select 3D-UMi NLOS for street canyon and 3D-UMi O2I for high-rise)
2. Select the NLOS propagation condition.
3. Calculate Omni-directional path-loss using [23]
   $PL[dB](d) = PL(d_0)dB + 10n_{pl}log_{10}(d) + \sigma_{SF}$

   Where $PL(d_0)dB$ is 296dB,n_{pl} is the path loss exponent (2.309), d is the distance in meters, and σ_{SF} is the shadow fading std (56.24) for NLOS.
4. Produce the large-scale parameters of rms delay spread, rms azimuth spread of arrival, rms elevation spread of arrival, etc., using table 4.23 to generate and cross-correlate them. Here, we generate five large-scale parameters and then correlate them. We limit AOA/AOD spread (ASA/ASD) to 100^0 and EOA/EOD (ESA/ESD) to 40^0.

5. Generate delays that are drawn from the delay distribution defined in Table 4.23 with Lognormal distribution. Calculate τ_n' where r_τ is the delay scaling factor given as 3. [7], σ_τ is the standard deviation of the distribution, and X_n is a unit-variance Gaussian RV

$$\tau_n' = -r_\tau \sigma_\tau ln X_n$$

We normalize the delays by subtracting the minimum delay from every other delay value and sort the result in descending order such that:

$$\tau_n = sort\left(\tau_n' - min(\tau_n')\right)$$

6. Produce the cluster power as:

$$P_n' = exp\left(-\tau_n \frac{r_\tau - 1}{r_\tau \sigma_\tau}\right).10^{-0.1Z_n}$$

Where $Z_n N(0, \beta^2)$, and β are the per cluster shadow fading term in dB given as 5 [7]. Normalize power such that the sum of all cluster power is one. i.e.

$$P_n = \frac{P_n'}{\sum_{n=1}^{N} P_n'}$$

7. Produce the azimuth angles of arrival and departure as shown below. The AOAs and AODs are governed by applying the inverse Gaussian function below with cluster power P_n and rms elevation spread of arrival and departure σ_{ASA} and σ_{ASD}, respectively, as input (after applying a scaling factor of 1.018 for 8 clusters). [22].

$$\varphi_{n,AOA} = 1.96(\sigma_{ASA}/1.4)\sqrt{-ln(P_n/max(P_n))}$$
$$\phi_{n,AOD} = 1.96(\sigma_{ASD}/1.4)\sqrt{-ln(P_n/max(P_n))}$$

8. Produce the elevation angles of arrival and departure as shown below. The EOAs and EODs are governed by applying the inverse Gaussian function below with cluster power P_n and rms elevation spread of arrival and departure σ_{ESA} and σ_{ESD}, respectively, as input (after applying a scaling factor of 1.104 for 12 clusters). [22].

$$\vartheta_{n,EOA} = -0.906\sigma_{EOA} ln\left(\frac{P_n}{max(P_n)}\right)$$
$$\theta_{n,EOD} = -0.906\sigma_{EOA} ln\left(\frac{P_n}{max(P_n)}\right)$$

9. Within a cluster, we couple all rays randomly, i.e., couple AOD, AOA, EOA, and EOD angles by randomizing the order of each group of angles within a cluster (e.g., using MATLAB's randperm (10) within each group of angles within a cluster).
10. Produce the cross-polarization power, XPRs as $\kappa_{l,n} = 10^{X/10}$ where X is Gaussian distributed.
11. Produce the random phase values for all four polarization combination terms, $\Phi_{l,n}^{vv}$, $\Phi_{l,n}^{vh}$, $\Phi_{l,n}^{hv}$, $\Phi_{l,n}^{hh}$. improves All parameters are compiled together in Table 3 for the simulation of channel reconstruction.

F. Reconstruction of 3D Channel Model of Lagos Island

In this section using the results of equation (11) – (24) and following the procedure in section E in the LTE tool in MATLAB, the 3D channel models presented in equation (25) to (28) below are reconstructed.

Street Canyon Line of Sight 3D model

$$H_{StreetCanyon}^{LOS}(t) = 0.3162H_{u,s,n}^{NLOS}(t) + \delta(n-1)0.9486\begin{bmatrix}-0.241.99\\ 1.330.96\end{bmatrix}^T \times \begin{bmatrix}e^{j\emptyset_{LOS}} & 0\\ 0 & e^{j\emptyset_{LOS}}\end{bmatrix} \times \begin{bmatrix}-0.513.36\\ 1.230.52\end{bmatrix} \quad (25)$$

Street Canyon Non-line of Sight 3D Model

$$H_{StreetCanyon}^{NLOS}(t;\tau) = \sqrt{\frac{P_n}{M}}\sum_{m=1}^{M_n}\begin{bmatrix}-0.241.99\\ 1.330.96\end{bmatrix}^T \begin{bmatrix}e^{j\emptyset_{n,m}^{\theta\theta}} & 0.33e^{j\emptyset_{n,m}^{\theta\varphi}}\\ 0.33e^{j\emptyset_{n,m}^{\varphi\theta}} & e^{j\emptyset_{n,m}^{\varphi\varphi}}\end{bmatrix} \times \begin{bmatrix}-0.513.36\\ 1.230.52\end{bmatrix} \quad (26)$$

High-rise Line of Sight 3D Model

$$H_{UrbanHighRise}^{LOS}(t) = 0.58H_{u,s,n}^{NLOS}(t) + \delta(n-1)0.82\begin{bmatrix}2.453.50\\ 0.200.12\end{bmatrix}^T \times \begin{bmatrix}e^{j\emptyset_{LOS}} & 0\\ 0 & e^{j\emptyset_{LOS}}\end{bmatrix} \times \begin{bmatrix}3.273.77\\ 0.220.25\end{bmatrix} \quad (27)$$

High-rise Non-line of Sight 3D Model

$$H_{UrbanHighRise}^{NLOS}(t;\tau) = \sqrt{\frac{P_n}{M}}\sum_{m=1}^{M_n}\begin{bmatrix}2.453.50\\ 0.200.12\end{bmatrix}^T \begin{bmatrix}e^{j\emptyset_{n,m}^{\theta\theta}} & 0.707e^{j\emptyset_{n,m}^{\theta\varphi}}\\ 0.707e^{j\emptyset_{n,m}^{\varphi\theta}} & e^{j\emptyset_{n,m}^{\varphi\varphi}}\end{bmatrix} \times \begin{bmatrix}3.273.77\\ 0.220.25\end{bmatrix} \quad (28)$$

V. SUMMARY AND CONCLUSION

Using the 3D LTE toolbox in MATLAB, we reconstructed bi-directional channel impulse response models otherwise called channel state information for LOS/NLOS of urban canyons and high rise in the 28 GHz mmWave band for Lagos Island Nigeria. These models are used to adequately assess competing air interface, random access channelization, and beam alignment procedures in mmWave systems. Future work will consider channel reconstruction in reconfigurable intelligent surfaces for cellular systems.

ACKNOWLEDGMENT

This work was supported by the Covenant Applied Informatics and Communication Africa Centre of Excellence (CApIC-ACE), Federated Genomic (FEDGEN) Research Cluster of Covenant University, the Covenant University Centre for Research, Innovation and Discovery (CUCRID), Nigeria and REMCOM Corporation State College, PA 16801 USA.

REFERENCES

[1] Q. Nadeem, S. Member, and A. Kammoun, "Elevation Beamforming with Full Dimension MIMO Architectures in 5G Systems : A Tutorial," pp. 1–31.

[2] O. Idowu-bismark and F. Idachaba, "5G Small Cell Backhaul : A Solution Based on GSM-Aided Hybrid Beamforming," no. August, pp. 24–31, 2019, doi: 10.5815/ijcnis.2019.08.03.

[3] O. Idowu-Bismark, F. Idachaba, and A. A. Atayero, "Large-scale parameter modeling for millimeter-wave multiple-input multiple-output channel in 5G ultra-dense network," Indones. J. Electr. Eng. Comput. Sci., vol. 26, no. 2, pp. 794–807, 2022, doi: 10.11591/ijeecs.v26.i2.pp794-807.

[4] O. Idowu-Bismark, F. Idachaba, and A. Atayero, "Massive MIMO Channel Characterization and Modeling: The Present and the Future," Int. J. Appl. Eng. Res. ISSN, vol. 12, no. 23, pp. 973–4562, 2017, [Online]. Available: http://www.ripublication.com

[5] O. B. Idowu-Bismark, A. E. Ibhaze, and A. A. Atayero, "Mimo Optimization Techniques and Their Application in Maximizing Throughput for 3GPP HSPA+," J. Wirel. Netw. Commun., vol. 7, no. 1, pp. 1–8, 2017, doi: 10.5923/j.jwnc.20170701.01.

[6] O. Idowu-Bismark, O. Kennedy, R. Husbands, and M. Adedokun, "5G wireless communication network architecture and its key enabling technologies," Int. Rev. Aerosp. Eng., vol. 12, no. 2, 2019, doi: 10.15866/irease.v12i2.15461.

[7] T. A. Thomas and H. C. Nguyen, "3D mmWave Channel Model Proposal," 2014.

[8] A. Tkac and V. Wieser, "Channel Estimation Using Measurement of Channel Impulse Response," no. May, 2014, doi: 10.1109/ELEKTRO.2014.6847883.

[9] R. Zhang, X. Lu, J. Zhao, L. Cai, and J. Wang, "Measurement and modeling of angular spreads of three-dimensional urban street radio channels," IEEE Trans. Veh. Technol., vol. 66, no. 5, pp. 3555–3570, 2017, doi: 10.1109/TVT.2016.2604394.

[10] Q. U. A. Nadeem, A. Kammoun, and M. S. Alouini, "Elevation Beamforming with Full Dimension MIMO Architectures in 5G Systems: A Tutorial," IEEE Commun. Surv. Tutorials, vol. 21, no. 4, pp. 3238–3273, 2019, doi: 10.1109/COMST.2019.2930621.

[11] C. Seker, M. T. Guneser, and H. Arslan, "Millimeter-wave propagation modeling and characterization at 32 GHz in indoor office for 5G networks," Int. J. RF Microw. Comput. Eng., vol. 30, no. 12, pp. 1–12, 2020, doi: 10.1002/mmce.22455.

[12] M. Kyrö, V. M. Kolmonen, and P. Vainikainen, "Experimental propagation channel characterization of mm-wave radio links in urban scenarios," IEEE Antennas Wirel. Propag. Lett., vol. 11, pp. 865–868, 2012, doi: 10.1109/LAWP.2012.2210532.

[13] S. G. Larew, T. A. Thomas, M. Cudak, and A. Ghosh, "Air interface design and ray tracing study for 5G millimeter wave communications," 2013 IEEE Globecom Work. (GC Wkshps), pp. 117–122, 2013, doi: 10.1109/GLOCOMW.2013.6824972.

[14] S. Hur et al., "Proposal on millimeter-wave channel modeling for 5G cellular system," IEEE J. Sel. Top. Signal Process., vol. 10, no. 3, pp. 454–469, 2016, doi: 10.1109/JSTSP.2016.2527364.

[15] C. Fan, X. Zhong, and J. I. E. Wei, "BS-to-Ground Channel Reconstruction With 3D Obstacle Map Based on RSS Measurements," vol. 7, pp. 99633–99641, 2019.

[16] S. S. Bujari, S. Ece, and B. Ece, "A Survey and Theoretical View on Compressive Sensing and Reconstruction," no. April, pp. 1–8, 2016, doi: 10.5815/ijigsp.2016.04.01.

[17] N. Prasad and X. F. Qi, "Channel Reconstruction in Intelligent Surface Aided Communications," vol. 2061, pp. 531–539.

[18] T. S. Rappaport et al., "Millimeter wave mobile communications for 5G cellular: It will work!" IEEE Access, vol. 1, pp. 335–349, 2013, doi: 10.1109/ACCESS.2013.2260813.

[19] P. F. M. Smulders and L. M. Correia, "Characterisation of propagation in 60 GHz radio channels," Electron. Commun. Eng. J., vol. 9, no. 2, pp. 73–80, 1997, doi: 10.1049/ecej:19970204.

[20] X. Y. Wang, B. Li, X. Yuan, J. W. Dou, and Y. Li, "Elevation angle research in three-dimension channel model using ray-tracing," 2014 31th URSI Gen. Assem. Sci. Symp. URSI GASS 2014, no. i, pp. 3–6, 2014, doi: 10.1109/URSIGASS.2014.6929281.

[21] R. N. Almesaeed, A. S. Ameen, E. Mellios, A. Doufexi, and A. Nix, "3D channel models: Principles, characteristics, and system implications," IEEE Commun. Mag., vol. 55, no. 4, pp. 152–159, 2017, doi: 10.1109/MCOM.2017.1500505.

[22] T. Specification, G. Radio, and A. Network, "3gpp tr 36.873," vol. 0, no. Release 12, 2014.

[23] S. K. Hinga and A. A. Atayero, "Deterministic 5G mmWave Large-Scale," IEEE Access, vol. PP, p. 1, 2021, doi: 10.1109/ACCESS.2021.3114771.